Check for updates

Naphthalenediimide-based nanoarchitectonics for a fluorescent chemosensor with highly selective and sensitive detection of cyanide ions†

Vilas K. Gawade,[a] Ratan W. Jadhav,[b] Vishnu R. Chari,[b] Rahul V. Hangarge[c] and Sheshanath V. Bhosale [ID] *[a]

A naphthalenediimide (NDI)-based highly potential chemosensor for the detection of cyanide has been synthesized successfully in several steps. The NDI-based probe displayed high selectivity and sensitivity towards cyanide ions in fluorescence 'turn-off' mode over other ions used in this study. The naked-eye, UV-vis absorbance and fluorescence methods are employed to investigate the sensing performance of probe **1** toward CN^- ion detection. The limit of detection for CN^- ions was calculated to be 4.11×10^{-7} M. Moreover, the Stern–Volmer quenching constant and fluorescence quenching efficiency of CN^- ions were estimated to be 1.1×10^5 M and 88.81%, respectively. Job's plot showed a 1 : 1 stoichiometric complexation reaction between probe **1** and CN^- ions. For practical applications, probe **1** was efficiently applied for the detection of CN^- ions using a paper strip method.

1 Introduction

Many ions are associated directly and indirectly with living organisms, but their excess may cause disturbances in the life cycle of the organisms.[1–3] Cyanide is considered to be one of the hazardous ions due to its toxicity[4] and strong binding to cytochrome P450.[5] Also, it is a serious threat to human beings due to its effects on the central nervous system.[1,6,7] The use of CN salt in various industries introduces CN into the environment *via* water and other factors; therefore, cyanide could enter the human body easily through water.[8]

Considering the significant threat of CN to living systems[9] many techniques and methods are emerging to detect cyanide.[10] The detection methods include the coordination mechanism,[11–13] hydrogen bonding interactions[14,15] deprotonation approach,[16] fluorescence phenomenon,[17,18] and nucleophilic addition reactions.[19–21] Out of these nucleophilic addition to the targeted molecule is a superior method[22] compared to the others due to the nucleophilic nature of cyanide and selective binding to the targeted molecule. These methods are executed with chromophores such as oxazine, pyrylium, acyltriazine, acridinium, squaraine, carbazole tetraphenylethene (TPE) dibenzothiophene, naphthalene diimide (NDI) coumarin and so on as a base unit.[23–25]

[a]*Department of Chemistry, School of Chemical Sciences, Central University Karanataka, Kalaburagi, Karanataka-585367, India. E-mail: svbhosale@unigoa.ac.in*
[b]*School of Chemical Sciences, Goa University, Taleigao Plateau, Goa-403 206, India*
[c]*Deaparment of Chemistry, Tai Gowalkar Mahavidyalaya, Ramtek, Nagpur-441106, India*

† Electronic supplementary information (ESI) available. See DOI: https://doi.org/10.1039/d3ay00615h

The chromophore has some limitations in selectivity, requiring a complex synthetic strategy, and long duration for the detection of cyanide ions. So, to find reactive chromophores is a challenge for researchers. In contrast, NDI has superior colorimetric, UV-vis, and emission response which is achieved by manipulating its core with different functionalities. Until now, NDI has been more explored in the sensing of anions, cations, pH, biosensors, *etc.*[25,26] Herein, we have reported NDI core-based simple and efficient molecular probe **1**, prepared in several steps starting from NDA **2**, for the selective and sensitive detection of CN^- ions, as shown in Scheme 1.

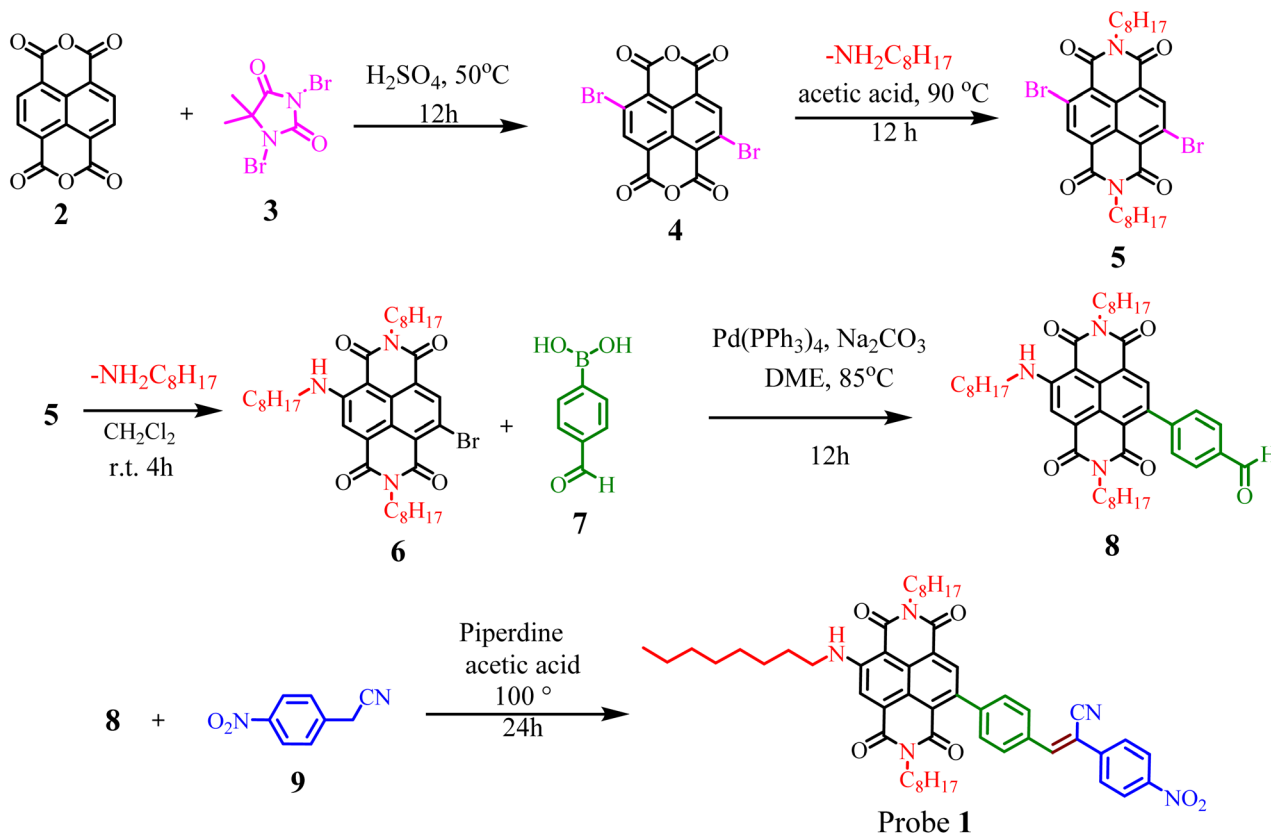## 2 Experimental details

2.1 Reagents and materials

Compounds **4**, **5**, and **6** were obtained through the procedure reported in the literature.[27] Compound **8** was prepared by the Suzuki coupling reaction between compounds **6** and **7**. And the final probe NDI **1** was synthesized by reacting compound **8** with compound **9** in the presence of piperidine and acetic acid as a solvent. Several anions of tetrabutylammonium salts (Cl^-, I^-, F^-, Br^-, HSO_4^-, $H_2PO_4^-$, NO_3^-, ClO_4^- and CN^-), chloroform, acetic acid, dichloromethane, piperidine, and THF were purchased from Sigma-Aldrich and TCI. ^{1}H NMR spectra and ^{13}C NMR spectra were recorded at 400 MHz using a 100 MHz Bruker spectrometer with tetramethylsilane (TMS) as an internal standard. $CDCl_3$-d was used as a deuterated solvent. UV-vis spectra were recorded using a UV-vis-1800 Shimadzu spectrophotometer, and fluorescence emission was measured on an Agilent Carry Eclipse spectrofluorophotometer.

Scheme 1 Synthetic route for probe **1**.

2.2 Sensing of anions

The detection of anions was conducted in chloroform at room temperature. The stock solution of probe **1** was prepared in 10^{-3} M and used for the sensing experiments with appropriate dilution in chloroform. A 10^{-3} M stock solution of anions was prepared in chloroform and used for the sensing experiments with appropriate dilution in chloroform. The UV-vis absorption and fluorescence emission spectra of probe NDI **1** in chloroform were measured in the presence and absence of anions. The absorption and emission spectra of probe **1** with different ions were recorded in chloroform at room temperature.

2.3 UV-vis absorption and fluorescence experiments

UV-vis absorption and fluorescence experiments of probe **1** were conducted upon the addition of 2 equiv. of anions. The 2 mL probe **1** (5×10^{-5} mol L^{-1}) in chloroform was placed in a quartz cell, and the UV-vis absorption and fluorescence spectra were recorded. Different anions (10×10^{-5} M) were added as salts, such as TBANO$_3$, TBAF, TBACN, TBAH$_2$PO$_4$, TBACl, TBABr, TBAI, TBAHSO$_4$, TBACN, and TBAClO$_4$. The UV-vis absorption and fluorescence emission spectra were recorded at room temperature.

2.4 UV-vis absorption and fluorescence titration of probe 1 upon the addition of CN⁻ ions

The 2 mL probe **1** (5×10^{-5} mol L^{-1}) in chloroform was placed in a quartz cell, and a fraction of TBACN (0–10×10^{-5} M) ion

solution was added, and the corresponding UV-vis absorption and fluorescence emission spectra of the probe NDI **1** were recorded at room temperature.

2.5 Naked-eye detection

The stock solution of the probe NDI **1** (5×10^{-3} mol L^{-1}) was prepared by dissolving it in chloroform solvent. Then various anions in salt forms such as TBANO$_3$, TBAF, TBACN, TBAH$_2$PO$_4$, TBACl, TBABr, TBAI, and TBAHSO$_4$ dissolved in chloroform (2×10^{-3} M) were added, and a photograph was taken under visible as well as 365 nm UV light.

3 Results and discussion

3.1 Synthesis and characterization of compound 1

Synthesis of probe **1** was achieved by a multistep reaction strategy, as shown in Scheme 1. In the first step, NDA (**2**) was reacted with dibromohydantoin (**3**) to obtain dibromo NDA (**4**), which on reaction with octyl amine in acetic acid, gives NDI **5**. The reaction of NDI **5** with octyl amine in DCM gives NDI **6**, which on Suzuki coupling with compound **7** gives NDI **8**. And finally, NDI **8** on condensation with compound **9** in acetic acid gives the molecular probe NDI **1**. All the synthesized compounds were characterized and confirmed by NMR spectroscopy, and the final compound was characterized by HRMS, as shown in Fig. S1 to S10.† Detailed experimental procedures are given in the ESI.†

3.2 Effect of polar solvent on the aggregation of 1

After successful synthesis and characterization, the behavior of NDI 1 was characterized in a mixture of non-polar and polar solvents, *i.e.*, THF/water with varying concentrations of water. For that, the UV-vis absorption and fluorescence spectra of NDI 1 were recorded in different proportions of THF/water solvent mixtures. The naked eye results showed that upon increasing the water proportion from 0 to 99%, a significant decrease in the fluorescence of NDI 1 was observed under visible as well as 365 nm UV light, as shown in Fig. 1a. In the UV-vis absorption spectra, the absorption band of probe NDI 1 in THF at 525 nm, due to the NDI core, was shifted to a higher wavelength as the water concentration increased from 0 to 99%, indicating the formation of J-aggregates, as shown in Fig. S11.† In the fluorescence spectra, NDI 1 shows high emission in THF at 571 nm wavelength when excited at 369 nm wavelength; upon increasing the water concentration from 0 to 99%, the emission intensity significantly decreases with a slight redshift, as shown in Fig. S11.† The decrease in the emission intensity is mainly due to the formation of J-aggregates of the NDI moiety at higher water concentrations. This significant decrease in the emission at 99% water fraction in THF indicates a strong ACQ behavior of NDI 1. The change in emission intensity with the % of water in THF is shown in Fig. 1b.

3.3 Solvatochromic study

To study solvatochromism, the UV-vis absorption and fluorescence emission spectra of NDI 1 were recorded in different solvents. In the UV-vis absorption spectra, NDI 1 showed almost similar absorption behavior in all solvents used with a small absorption shift. In the MCH solvent for NDI 1, the absorption band was observed at 522 nm wavelength, whereas in chloroform, the absorption band shifted to a higher wavelength at
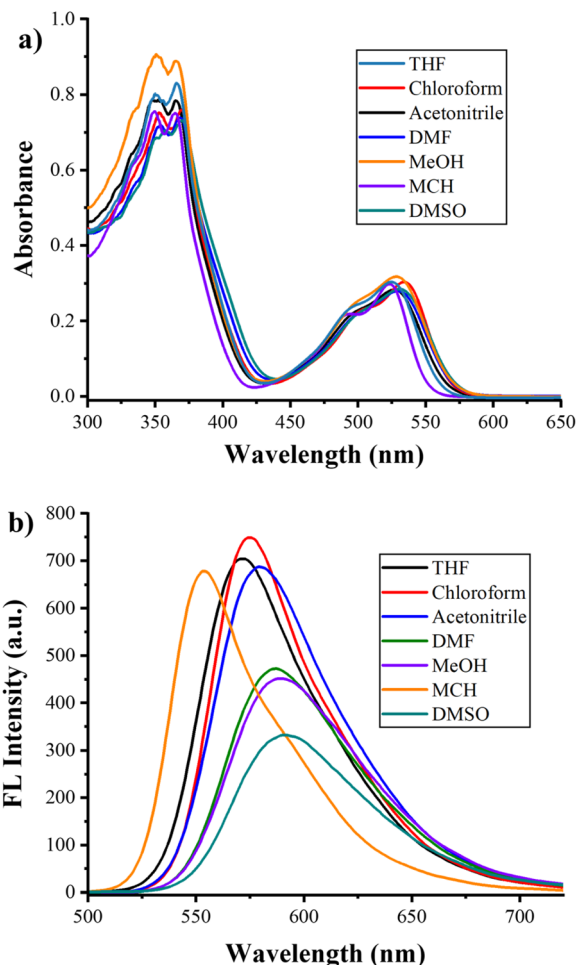

Fig. 2   (a) UV-vis absorption and (b) fluorescence emission spectra of NDI 1 in different solvents.
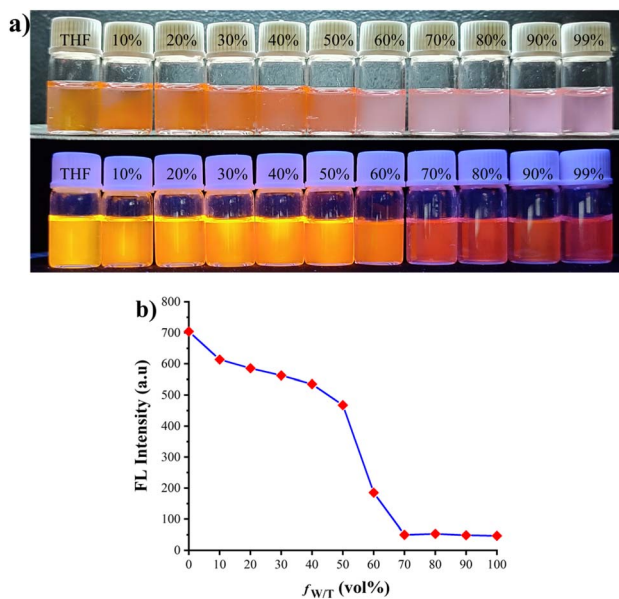

Fig. 1   (a) Picture of NDI 1 (5 × 10⁻⁵ M) in THF/H₂O mixtures with different f_w values (0 to 99%) under visible light and 365 nm UV light; (b) plot of relative fluorescence emission intensity as a function of f_w.

535 nm. Moreover, the highest absorbance of NDI 1 was observed in MeOH, whereas the lowest absorbance was in DMSO solvent, as shown in Fig. 2a. This behavior of NDI 1 in different solvents is mainly due to the solvatochromic effect and the solvation energy difference between the ground state and the excited state of the NDI 1 molecule.

Furthermore, the fluorescence spectra of NDI 1 were also recorded in different solvents. The NDI 1 molecule showed the highest emission in chloroform and the lowest emission in DMSO solvent. In MCH, NDI 1 showed blue shifted emission at 553 nm wavelength, whereas in the THF, chloroform, acetonitrile, DMF, MeOH, and DMSO the emission band was shifted towards higher wavelengths such as at 571, 575, 580, 586, 588, and 591 nm, as shown in Fig. 2b. Due to the solvatochromic effect, the NDI 1 molecule showed such different emission behaviors in different solvents.

4   Sensing performance of probe NDI 1

The sensing ability of NDI 1 towards various anions was characterized by naked-eye detection, UV-vis absorption spectroscopy, and fluorescence spectroscopy.

4.1 Naked eye detection

The stock solution of NDI **1** was prepared in chloroform and used for further sensing characterization. For the naked-eye detection study, a series of ions such as I^-, Br^-, Cl^-, F^-, CN^-, HSO_4^-, OAc^-, $H_2PO_4^-$, and ClO_4^- were added to the solution of NDI **1**, and the sensing performance was monitored by a visual color change in visible as well as 365 nm UV light. Under visible light, it was observed that the orange color of the solution changed to brown only in the presence of CN^- ions, whereas when other ions were used, it did not show any changes, as shown in Fig. 3. Also, under 365 nm UV light, the light orange fluorescence of NDI **1** was quenched only in the presence of CN^- ions, whereas other ions used did not show such fluorescence quenching. These naked eye results suggested that NDI **1** can be used as a chemosensor for the selective and sensitive detection of CN^- ions.

The sensing performance of NDI **1** towards the CN^- ion was further characterized by UV-vis absorption and fluorescence emission spectroscopy.

4.2 UV-vis absorption

UV-vis spectroscopy was used to investigate the sensing ability of NDI **1** towards the tetrabutyl ammonium salts of I^-, Br^-, Cl^-, F^-, CN^-, HSO_4^-, OAc^-, PO_4^-, and ClO_4^- ions (2 equivalents). The UV spectra of NDI **1** were recorded in chloroform solvent before and after the addition of ions. In the UV-vis absorption spectra, NDI **1** exhibited four absorption bands at 269, 353, 369, and 533 nm, which were used to monitor the sensing performance of probe NDI **1**. After the addition of all the above-mentioned ions to the probe solution, a significant change in the UV spectrum of probe NDI **1** was observed only with the CN^- ion. The absorption bands at 353 and 369 nm disappeared, and the absorption band at 533 nm blue shifted to 513 nm, indicating the formation of H-aggregates of probe NDI **1** in the presence of CN^- ions. The other ions used showed a very insignificant effect on the UV-vis absorption spectrum of probe NDI **1**. These results suggest that the probe NDI **1** is highly selective towards CN^- ions. The nucleophilic addition of CN^- ions takes place with probe NDI **1**. The addition of CN^- occurs at the double bond in conjugation with cyanide, which results

in changes in the absorption spectrum, as shown in Fig. 4a. For a detailed understanding, the probe NDI **1** was titrated with two equivalents of CN^- ions in chloroform solution. The titration experiments clearly show that upon incremental addition of CN^- ions into the NDI **1** solution, the absorption bands at 353 and 369 nm slowly disappear, and the absorption band at 533 nm gradually shifts towards a lower wavelength, as shown in Fig. 4b. Hence, these UV-vis absorption changes clearly show that the probe NDI **1** is an excellent candidate for selective sensing of CN^- ions.

4.3 Fluorescence study

Furthermore, the fluorescence emission spectra were employed to investigate the sensing performance of probe NDI **1** in chloroform. The fluorescence spectra of NDI **1** were recorded before and after the addition of I^-, Br^-, Cl^-, F^-, CN^-, HSO_4^-, OAc^-, $H_2PO_4^-$, and ClO_4^- ions (2 equivalents) at room temperature. When excited at 368 nm wavelength, fluorescent probe NDI **1** exhibited an intense emission band at 575 nm wavelength in chloroform, which was used to monitor the sensing ability of probe **1** towards the series of ions. It was clearly observed that the quenching of fluorescence of probe **1**
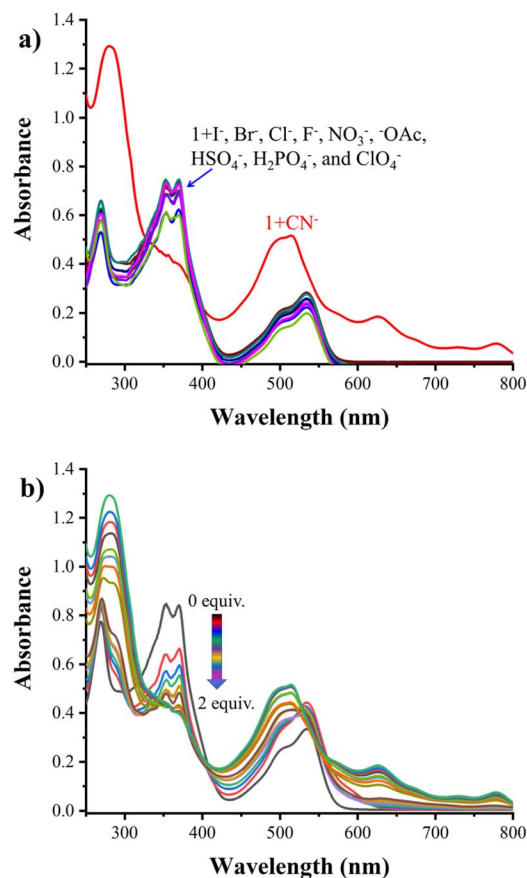

Fig. 4 UV-vis absorption spectra of probe **1** (5×10^{-5} M) in the presence of (a) 2 equiv. of CN^-, I^-, Br^-, Cl^-, F^-, NO_3^-, OAc^-, HSO_4^-, $H_2PO_4^-$, and ClO_4^- (10×10^{-5} M) as tetrabutylammonium salts. (b) Addition of the tetraethylammonium salt of CN^- (0 to 10×10^{-5} M) in chloroform.

Fig. 3 Solutions of probe **1** in chloroform; blank is without any anions and respectively with the addition of **2** equivalents of tetrabuty-lammonium salts of CN^-, I^-, Br^-, Cl^-, F^-, NO_3^-, OAc^-, HSO_4^-, $H_2PO_4^-$, and ClO_4^- with probe **1**: (a) under visible light and (b) under 365 nm UV light.

occurs only in the presence of CN$^-$ ions, whereas there was no noticeable change observed in the fluorescence spectra of probe **1** with the other ions used, as shown in Fig. 5a. The intense emission band of probe **1** decreases dramatically, and the intensity of probe **1** decreases from 575 nm to 569 nm after the addition of CN$^-$ ions. These results further support the fact that probe **1** is highly selective towards the CN$^-$ ion. The nucleophilic addition of a CN$^-$ ion to the double bond conjugated to cyanide results in such a quenching of the fluorescence of the probe **1**. Furthermore, the fluorescence titration experiments were carried out upon incremental addition of CN$^-$ ions (2 equivalents) to the solution of probe **1**, to get deep insights and to calculate the detection limit. Upon incremental addition of CN$^-$ ions (0 to 2 equivalents), the emission intensity of probe **1** gradually decreased from 575 nm to 569 nm, and further addition of CN$^-$ ions did not show any changes in the fluorescence spectrum, as shown in Fig. 5b. The quantum yield of probe **1** also decreased from 64% to 7.9% after the addition of CN$^-$ ions.

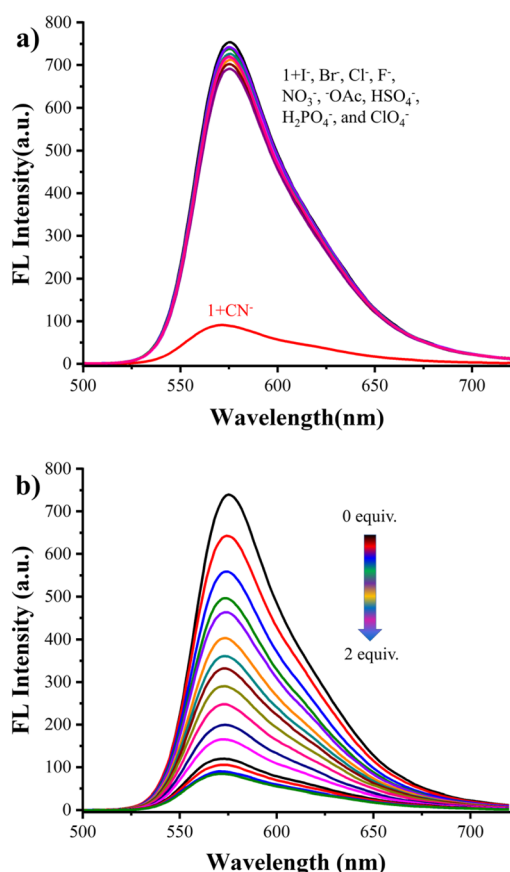The initial fluorescence intensity of probe **1** was found to be significantly decreased upon incremental addition of the CN$^-$ ion. Therefore, fluorescence quenching efficiency (η) was calculated using the following equation:

$$[(I_0 - I)/I_0] \times 100\%$$

where I and I_0 are the fluorescence intensities after and before the addition of the CN$^-$ ions; after the addition of 2 equivalent of CN$^-$ ions, the emission intensity of probe **1** was quenched approximately up to 88.81%, and the quenching efficiency (η) was calculated to be about 88.81%.

The sensing performance of probe **1** was studied at different pH values and the results are depicted in Fig. S15.† At pH 4 there is no difference in the fluorescence intensity after and before addition of CN ions, whereas at pH 7 and 9.2 the fluorescence intensity of probe **1** decreases upon addition of CN ions.

4.4 Selectivity study of probe 1 for CN$^-$ ions

To evaluate the selectivity study of probe **1** towards cyanide, the fluorescence emission response of probe **1** with various ions such as I$^-$, Br$^-$, Cl$^-$, F$^-$, CN$^-$, HSO$_4^-$, OAc$^-$, H$_2$PO$_4^-$, and ClO$_4^-$ (2 equivalents) was investigated. Probe **1** showed a significant response to the CN$^-$ ion only, and the other ions used showed insignificant effects, as shown in Fig. S12.† It clearly indicates selective detection of CN$^-$ ions over other anions used.

4.5 Competitive CN$^-$ ion binding

To explore the specificity of probe **1** as a CN$^-$ selective fluorescence sensor, the competitive experiments of probe **1** were performed by using various anions (2 equiv.) as an interfering anion. As depicted in Fig. 6, the red bar corresponds to probe **1** with the tested anions (F$^-$, Cl$^-$, Br$^-$, I$^-$, HSO$_4^-$, H$_2$PO$_4^-$, OAc$^-$, NO$_3^-$, and ClO$_4^-$), whereas the blue bar corresponds to probe **1** with one of the tested anions in the presence of CN$^-$ ions. It was observed that CN$^-$ could diminish the fluorescence of probe **1** in the presence of other anions. These results strongly indicate that the tested anions have no effect on
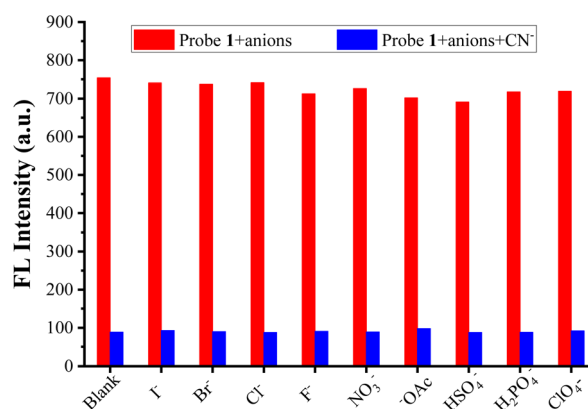

Fig. 5 Fluorescence emission spectra of probe **1** (5 × 10^{-5} M) in the presence of (a) 2 equiv. of CN$^-$, I$^-$, Br$^-$, Cl$^-$, F$^-$, NO$_3^-$, OAc$^-$, HSO$_4^-$, H$_2$PO$_4^-$, and ClO$_4^-$ (10 × 10^{-5} M) as tetrabutylammonium salts. (b) Addition of the tetraethylammonium salt of CN$^-$ (0 to 10 × 10^{-5} M) in chloroform.

Fig. 6 Competitive binding interactions of CN$^-$ ions (2 equiv.) with probe **1** in presence of interfering anions (2 equiv.) (λ_{ex} = 369 nm). The red bar represents probe **1** + other anions and blue bar represents probe **1** + other anions + CN$^-$ ion.

probe **1** for CN⁻ ion detection. Hence, probe **1** can be employed as a fluorescence sensor with excellent selectivity for CN- ion detection.

4.6 Time-correlated single photon counting (TCSPC) studies

The fluorescence decay time displays a dynamic picture of the obtained fluorescence, which is independent of the concentration of the solution. The time correlated single photon counting (TCSPC) method was used to study the kinetics of the emission *via* optical excitation of the samples, individual photon arrival time, and their detection. TCSPC of probe **1** and probe **1** + CN in chloroform with excitation at 376 nm and emissions was recorded at 413 nm, respectively (Fig. 7). Decay profiles of probe **1** and probe **1** + CN were fitted with bi-exponential functions. In chloroform solutions, for probe **1**, the fluorescence lifetime was 7.58 ns, and the fluorescence lifetime of probe **1** + CN was 7.88 ns.

4.7 Sensing mechanism of probe 1

Probe NDI **1** is composed of an NDI fluorophore and a nitro-phenylacetonitrile-containing doubly activated Michael acceptor for a cyanide anion (Fig. 8), and this molecular design makes probe **1** possess extended *p*-conjugation as well as the strong intramolecular charge transfer (ICT) from NDI bearing three long alkyl chains to the conjugated nitro-phenylacetonitrile moiety, which will lead to the quenching of
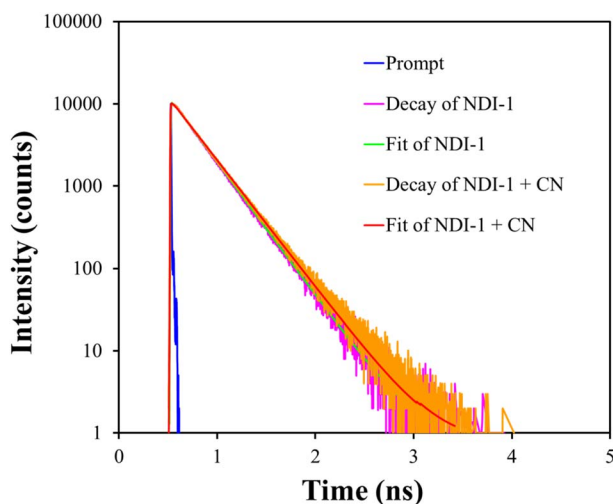

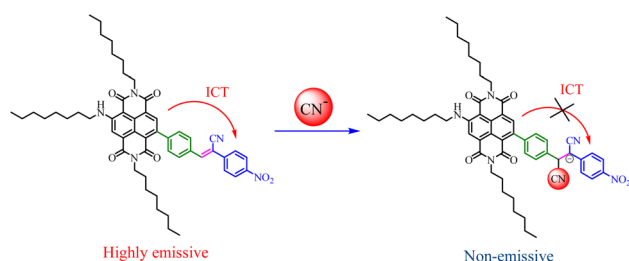Fig. 7 TCSPC measurements of probe **1** with and without CN.

Fig. 8 Sensing mechanism of probe NDI **1** towards CN⁻ ions.

the orange fluorescence of probe **1**. It is expected that a CN⁻ ion can add to the *b*-position of the activated Michael acceptor to produce the stabilized anionic species probe **1** + CN ion.[28] Most importantly, this addition reaction blocks the ICT due to interruption of the conjugation, due to which a hypsochromic shift in the absorption and emission of NDI moiety is observed.

The sensing of CN ions was also characterized by IR spectroscopy. Herein, the band near 2250 cm⁻¹ increased after addition of CN⁻ to the probe as shown in Fig. S16.† There are also changes and addition of many bands in the fingerprint region in the spectrum of probe **1** + CN⁻ which clearly indicates the addition of CN⁻ to the double bond nucleophilically.

4.8 Density functional theory (DFT) study

To understand the reactivity of **1** towards CN⁻ ions, DFT calculations were performed. The geometry optimization was carried out at the B3LYP/6-31+G(d,p) level of theory and was corrected for solvent effects using the continuum solvation model and chloroform as solvent. Frequency calculations were performed to verify that the optimized structure was not in a transition state. All the calculations were performed using the Gaussian 16 software package. The condensed dual descriptor (CDD) for **1** was calculated using Multiwfn software. A positive CDD value suggests that the atom will undergo nucleophilic attack, whereas an atom with a negative CDD value favors electrophilic attack. Fig. 9 shows the isosurface of CDD for **1**. The lime green colored blob indicated a positive isosurface at 0.001 isovalue and the orange isosurface indicates a negative isosurface. The CDD value for *C* adjacent to the cyano group is positive (0.0101 units) and suggests that this carbon is one of the most favorable sites for nucleophilic attack,[1] which is in agreement with the experimental results. The frontier molecular orbitals (FMO) of **1** and **1** + CN⁻ were generated at an isovalue of 0.03 using Chemcraft and are presented in Table S2.† The highest occupied molecular orbital (HOMO) of **1** is prominently located on the aromatic ring system and for **1** + CN⁻ it is on the aromatic ring of the cyano group-containing subunit, respectively. The lowest unoccupied molecular orbital (LUMO) in **1** is located primarily on the aromatic ring
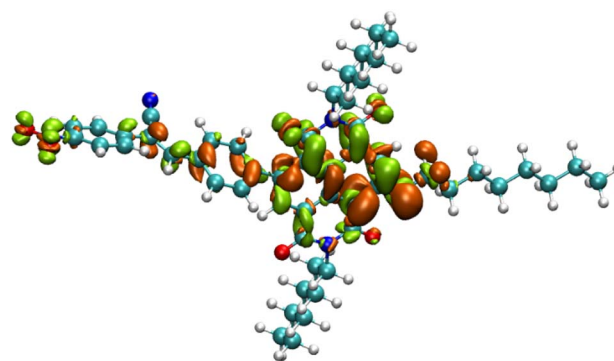

Fig. 9 CDD isosurface of the **1** lime-green blob represents the positive value and that of the orange blob represents the negative value of CDD for a given atom.

system, whereas for **1** + CN$^-$ the electron density shifts towards the aromatic ring from the cyano group-containing subunit. This results in the change of band gap for **1** from 2.75 eV (corresponding to a λ_{max} of 450 nm) to 1.33 eV for **1** + CN$^-$ (corresponding to a λ_{max} of 932 nm).

Fig. 11 Paper strip based selective detection of CN$^-$ ions with probe NDI-**1**, over other anions by the naked eye under 365 nm UV light.

4.9 Stern–Volmer quenching constant and limit of detection

The Stern–Volmer quenching constant (K_{sv}) for a CN$^-$ ion was calculated by using fluorescence emission intensity of probe **1** (I_0/I) as a function of increasing CN$^-$ ion concentration [Q] by using the equation I_0/I = probe **1** + K_{sv} [Q], where I and I_0 are the emission intensities of probe **1**, with and without the addition of CN$^-$ iond, respectively, K_{sv} is the quenching constant (M^{-1}), and [Q] is the concentration of CN$^-$ ions in a mole. The Stern–Volmer plot of probe **1** with CN$^-$ ions is depicted in Fig. 10a, where it can be seen that the Stern–Volmer plot showed a good linearity at low concentrations of CN$^-$ ions (4 × 10^{-5} M), whereas at higher concentrations, the linearity slightly deviated in the upward direction. The K_{sv} value obtained for CN$^-$ ions using probe **1** was 1.1 × 10^5 M^{-1}. These results indicate that the CN$^-$ ion exhibited exclusive quenching ability towards fluorescent probe **1** in chloroform.

The detection limit was evaluated using fluorescence emission titration of probe **1** with CN$^-$ ions in chloroform, which
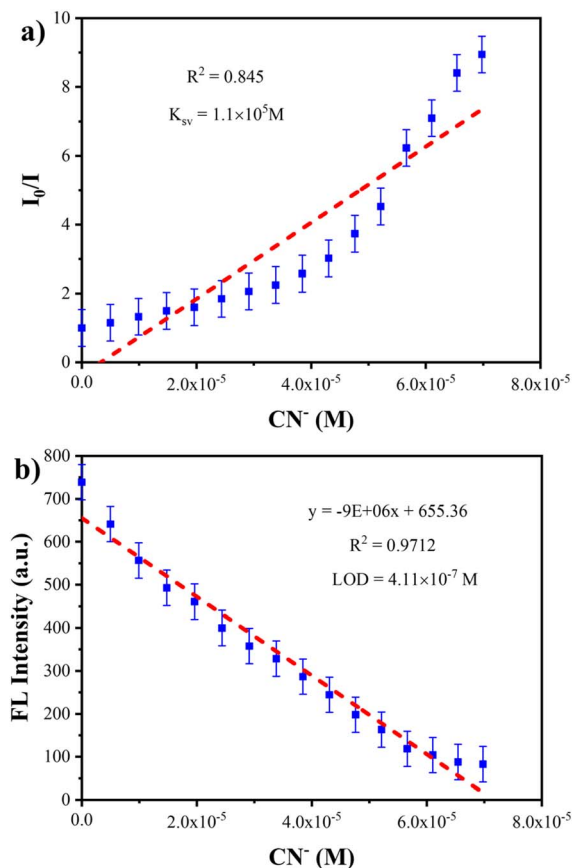
was carried out by adding increasing concentrations of CN$^-$ ion solution (2 equivalents), and the emission intensity as a function of CN$^-$ ion added was then plotted as shown in Fig. 10b. The detection limit was calculated by using the equation Detection limit = $3\sigma/m$, where σ is the standard deviation of the fluorescence emission of the free probe, and m is the slope between emission at 575 nm and the CN$^-$ ion concentration. The detection limit for the CN$^-$ ion was calculated to be 4.11 × 10^{-7} M in chloroform showing the fluorescence intensity of probe **1** at 575 nm (λ_{ex} = 369 nm) as a function of the concentration of CN$^-$ ions. Hence the detection limit of probe **1** in chloroform was found to be 4.11 × 10^{-7} M which is comparable with that of other molecules used for the detection of CN$^-$ ions (Table S2†).

4.10 Stoichiometry and binding constant

To investigate the binding of probe **1** and CN$^-$ ions, the Job plot was analyzed. The plot of changes in fluorescence emission intensity **1**/[I_0 − I] against the molecular fraction of [**1**]/[**1** + CN$^-$] is depicted in Fig. S12a.† The Job's plot results suggest a 1 : 1 stoichiometric complexation between probe **1** and CN$^-$ ions.

Furthermore, the Benesi–Hildebrand plot (Fig. S12b†), was used to describe the binding constant (K_a) of probe **1** for CN$^-$ ions. The linear relationship of fluorescence emission intensity as a function of **1**/[CN$^-$] was found to be 2 × 10^4 M. This result proposes that probe **1** has a strong binding affinity towards CN$^-$ ions.

Cyanide is nucleophilic in nature. It attacks the electrophilic center of the double bond. This nucleophilic nature of cyanide is utilized by many researchers for cyanide detection as indicated in Table S2.† Amongst, few derivatives show good limit of detection (LOD), however, have problems with for real-world applications like test strip-based sensing. Important to mention, NDI-**1** not only having a lower limit of detection value but also shown to be useful for real world applications such as test strip sensing.

4.11 Test strip for CN$^-$ detection using probe 1

For practical application, a test strip was employed for CN$^-$ ions. For this, the test strip was prepared using a chloroform solution of probe **1** and the detection of CN$^-$ ions was performed. The results are presented in Fig. 11. The test paper of probe **1** is orange in color under 365 nm UV light, and it was observed that the orange color of probe **1** disappeared only in the presence of CN$^-$ ions, whereas the other anions used did not display such an effect.

Fig. 10 a) Stern–Volmer plot for probe **1** with CN$^-$ ions; (b) plot for the determination of the limit of detection for CN$^-$ ions.

5 Conclusion

A new highly selective chemosensor based on electron rich aromatic naphthalene diimide (NDI) has been designed, synthesized and utilised for the detection of cyanide ions. The NDI-based sensor shows high selectivity and sensitivity toward cyanide ions with "turn-off" fluorescence emission. Nonetheless, observation by the naked eye under UV (365 nm) and visible light, and furthermore, UV-vis absorbance spectroscopy clearly show cyanide detection with the simple probe **1**. FT-IR spectroscopy was used to evaluate addition of a cyanide ion to the double bond of probe **1**; thus, the addition of cyanide to the double bond shows irreversibility even through changes in pH *i.e.* acidic/basic. Briefly, a pH dependent study with the addition of cyanide ions was also conducted and shows no influence of the acidic environment; however, upon making it too basic, complete fluorescence quenching occurred upon addition of cyanide to probe **1**. A significant outcome to mention is that the limit of detection of the cyanide ion with probe **1** was calculated to be 4.11×10^{-7}, with the Job plot showing a 1 : 1 stoichiometric complex. Furthermore, we have shown the paper strip method of the sensing mechanism of probe **1** upon addition of cyanide ions step-wise, which is a very significant phenomenon for practical applications.

Author contributions

V. K. G., R. W. J. and R. V. H. performed synthesis, characterization, sensing experiments and prepared first draft of the manuscript. V. R. C. performed DFT calculations. S. V. B. interpreted and analyzed the data and finalized the manuscript. All co-authors reviewed the manuscript.

Conflicts of interest

The authors declare no competing interests.

Acknowledgements

References

1 Q. Lin, L. Liu, F. Zheng, P. P. Mao, J. Liu, Y. M. Zhang, H. Yao and T. B. Wei, *RSC Adv.*, 2017, **7**, 38458–38462.

2 R. Martínez-Máñez and F. Sancenón, *Chem. Rev.*, 2003, **103**(11), 4419–4476.

3 F. P. Schmidtchen and M. Berger, *Chem. Rev.*, 1997, **97**, 1609–1646.

4 G. A. Zalmi, V. K. Gawade, D. N. Nadimetla and S. V. Bhosale, *ChemistryOpen*, 2021, **10**, 681–696.

5 G. A. Zalmi, D. N. Nadimetla, P. Kotharkar, A. L. Puyad, M. Kowshik and S. V. Bhosale, *ACS Omega*, 2021, **6**, 16704–16713.

6 N. Busschaert, C. Caltagirone, W. Van Rossom and P. A. Gale, *Chem. Rev.*, 2015, **115**, 8038–8155.

7 S. V. Krivovichev, O. Mentré, O. I. Siidra, M. Colmont and S. K. Filatov, *Chem. Rev.*, 2013, **113**, 6459–6535.

8 Y. Kim, H. S. Huh, M. H. Lee, I. L. Lenov, H. Zhao and F. P. Gabbaï, *Chem.–Eur. J.*, 2011, **17**, 2057–2062.

9 J. Ma and P. K. Dasgupta, *Anal. Chim. Acta*, 2010, **673**, 117–125.

10 E. Palomares, M. Victoria Martínez-Díaz, T. Torres and E. Coronado, *Adv. Funct. Mater.*, 2006, **16**, 1166–1170.

11 Y. Y. Guo, X. L. Tang, F. P. Hou, J. Wu, W. Dou, W. W. Qin, J. X. Ru, G. L. Zhang, W. S. Liu and X. J. Yao, *Sens. Actuators, B*, 2013, **181**, 202–208.

12 I. J. Kim, M. Ramalingam and Y. A. Son, *Sens. Actuators, B*, 2017, **246**, 319–326.

13 B. A. Rao, J. Y. Lee and Y. A. Son, *Spectrochim. Acta, Part A*, 2014, **127**, 268–274.

14 T. Wei, G. Wu, B. Shi, Q. Lin, H. Yao and Y. Zhang, *Chin. J. Chem.*, 2014, **32**, 1238–1244.

15 G. A. Zalmi, R. W. Jadhav, H. A. Mirgane and S. V. Bhosale, *Molecules*, 2022, **27**, 150.

16 Y. H. Jeong, C. H. Lee and W. D. Jang, *Chem.–Asian J.*, 2012, **7**, 1562–1566.

17 N. Kumari, S. Jha and S. Bhattacharya, *Chem.–Asian J.*, 2014, **9**, 830–837.

18 E. Jeong, S. Yoon, H. S. Lee, A. Kumar and P. S. Chae, *Dyes Pigm.*, 2019, **162**, 348–357.

19 M. Dong, Y. Peng, Y. M. Dong, N. Tang and Y. W. Wang, *Org. Lett.*, 2012, **14**, 130–133.

20 R. Guliyev, S. Ozturk, E. Sahin and E. U. Akkaya, *Org. Lett.*, 2012, **14**, 1528–1531.

21 J. Jo, A. Olasz, C. H. Chen and D. Lee, *J. Am. Chem. Soc.*, 2013, **135**, 3620–3632.

22 V. G. More, D. N. Nadimetla, D. B. Shaikh, A. L. Puyad, S. V. Bhosale and S. V. Bhosale, *ChemistrySelect*, 2022, 7, 6–11.

23 P. B. Pati, *Sens. Actuators, B*, 2016, **222**, 374–390.

24 M. T. Gabr and F. C. Pigge, *Dalton Trans.*, 2018, **47**, 2079–2085.

25 S. V. Bhosale, M. Al Kobaisi, R. W. Jadhav, P. P. Morajkar, L. A. Jones and S. George, *Chem. Soc. Rev.*, 2021, **50**, 9845–9998.

26 V. G. More, D. N. Nadimetla, G. A. Zalmi, V. K. Gawade, R. W. Jadhav, Y. D. Mane and S. V. Bhosale, *ChemistryOpen*, 2022, **11**, 12–15.

27 M. Sasikumar, Y. V. Suseela and T. Govindaraju, *Asian J. Org. Chem.*, 2013, **2**, 779–785.

28 S. H. Kim, S. J. Hong, J. Yoo, S. K. Kim, J. L. Sessler and C. H. Lee, *Org. Lett.*, 2009, **11**, 3626–3629.